Journal of
Ceramic Science
and Technology

J. Ceram. Sci. Technol., **09** [2] 209-214 (2018)
DOI: 10.4416/JCST2018-00004
available online at: http://www.ceramic-science.com
© 2018 Göller Verlag

Short Communication

Room-Temperature Structural and Dielectric Properties of Praseodymium-Doped $SrBi_2Nb_2O_9$ Ceramics

M. Afqir*[1, 2], A. Tachafine[2], D. Fasquelle[2], M. Elaatmani[1], J.-C. Carru[2], A. Zegzouti[1]

[1]Laboratoire des Sciences des Matériaux Inorganiques et leurs Applications,
Faculté des Sciences Semlalia, Université Cadi Ayyad, Marrakech, Maroc
[2]Unité de Dynamique et Structure des Matériaux Moléculaires,
Université du Littoral- Côte d'Opale, Calais, France

received January 21, 2018; received in revised form February 22, 2018; accepted March 9, 2018

Abstract

In the present work, we studied the influence of substituting Pr for Bi on the structural and dielectric properties of $SrBi_{2-x}Pr_xNb_2O_9$ (x = 0, 0.2) ceramics at room temperature. The samples were prepared by the solid-state reaction method. The XRD patterns of the doped sample corresponded well with those of the undoped samples. SEM revealed that the Pr doping brings significant change to the microstructure. The results obtained from different experimental dielectrics at room temperature are correlated to discuss the structure-property relationship with consideration of the internal microstructure, the strengths of chemical bonds (Pr-O and Bi-O) and the oxidation of Pr^{3+} to Pr^{4+}. The dielectric constant increased with Pr-doping, while the dielectric loss decreased. Praseodymium is introduced into $SrBi_2Nb_2O_9$ to reduce the number of oxygen ion vacancies available for the conduction process.

Keywords: $SrBi_2Nb_2O_9$, Pr^{3+}/Pr^{4+}, crystal structure, dielectrics

I. Introduction

Bismuth layer-structured ferroelectrics (BLSFs) can be described as a regular intergrowth of $(Bi_2O_2)^{2+}$ layers with $(A_{m-1}B_mO_{3m+1})^{2-}$ perovskite-type layers. The general chemical formula for BLSFs is $(Bi_2O_2)^{2+}(A_{m-1}B_mO_{3m+1})^{2-}$, where A is mono-, di- or trivalent cations, B is a transition metal, and m is a number of post-perovskites $(A_{m-1}B_mO_{3m+1})^{2-}$.

$SrBi_2Nb_2O_9$ like $SrBi_2Ta_2O_9$, with its high Curie temperature and excellent resistance to fatigue, has been used in soldering materials for FeRAM applications. However, these materials suffer from high dielectric loss arising from volatilization of bismuth during the sintering process. The substitution of rare earth ions for Bi^{3+} ions resulted in a reduction in oxygen vacancies [1, 2, 3]. Recently, we have found that the substitution of Gd^{3+} ions for Bi^{3+} ions in $SrBi_{2-x}Gd_xNb_2O_9$ ($0 \le x \le 0.5$) ceramics significantly reduces dielectric loss [4]. Shiming Huang *et al.* [5] reported that $SrBi_{1.8}Pr_{0.2}Nb_2O_9$ ceramic exhibited a relaxor behavior of frequency dispersion. The substitution of Pr ions for Bi^{3+} ions resulted in a shift of the Curie temperature to lower temperatures, a decrease in remanent polarization and a reduction of the coercive field. Hua Zou *et al.* [6] reported that $SrBi_{2-x}Pr_xNb_2O_9$ ($0 \le x \le 0.03$) ceramics presented the red emission excited by ultraviolet light. The remanent polarization values of the hysteresis loops (P–E hysteresis loops) increased with increasing Pr content. Maximum dielectric constant and Curie temperature decreased with increasing Pr doping, while the dielectric loss did not change significantly. The lower shift of the Curie temperature and the better shapes of P–E hysteresis loops may be attributed respectively to the degree of structural distortion [7] and the elimination of oxygen vacancy and vacancy complex defects. For holmium-substituted $SrBi_{2-x}Ho_xTa_2O_9$ (x = 0.00 – 2.0), the compositions showed a single-phase layered perovskite structure formation for a holmium content up to $x \le 0.1$, the dielectric loss is reduced significantly with holmium substitution. The specimen with x = 0.01 exhibits highest remanent polarization (Pr = 9.22 $\mu C/cm^2$) while the bismuth-free specimen shows the lowest value of remanent polarization [8].

The experimental approach of this work is very similar to that described in our recently published papers Dielectric properties of $SrBi_{1.8}RE_{0.2}Nb_2O_9$ (RE = Yb, Tm, Tb, Gd, Er, Sm and Ce) ceramics [9] and Dielectric properties of gadolinium-doped $SrBi_2Nb_2O_9$ ceramics [4]. The material characterization results are mostly alike between the two papers except that the data were obtained from samples with slightly different compositions.

Despite that, there is a lack of data in respect of structural and electrical characterization of Pr-doped $SrBi_2Nb_2O_9$ materials. This manuscript describes a study of the doping effects of praseodymium ions on the structural dielectric properties at room temperature of $SrBi_{2-x}Pr_xNb_2O_9$ (x = 0, 0.2) ceramics.

* Corresponding author: mohamed.afqir@yahoo.fr

II. Experimental

$SrBi_{2-x}Pr_xNb_2O_9$ (x = 0, 0.2) ceramic powders were prepared with the solid-state reaction method, using Bi_2O_3, Nb_2O_5, $SrCO_3$, Pr_6O_{11} as raw materials. A stoichiometric ratio with Bi_2O_3-excess was ground in an agate mortar. The powders were pelletized into discs, measuring 6 mm in diameter and about 1 mm in thickness, which were then sintered at 1200 °C (x = 0) and 1230 °C (x = 0.2) for 12 h. Both sides of the sintered pellets were painted with silver paste and fired to form electrodes. X-ray diffraction (XRD) was performed with a Philips X'Pert Pro with CuK*a* radiation. The microstructure was analyzed with a JEOL JSM-840 scanning electron microscope (SEM). Dielectric measurements were conducted using a HP4284A impedance analyzer in the frequency range 1000 Hz – 1 MHz.

The value of AC conductivity was calculated using the formula:

$$\sigma_{ac} = \omega \varepsilon_0 \varepsilon' \tan\delta \qquad (1)$$

where ω is the angular frequency, ε' is dielectric constant, $\tan\delta$ is the dielectric loss tangent and ε_0 is the permittivity of free space.

The complex impedance of the samples was calculated using the relations:

$$Z' = \frac{1}{\omega C_0}\left[\frac{\varepsilon''}{\varepsilon'^2 + \varepsilon''^2}\right] \qquad Z'' = \frac{1}{\omega C_0}\left[\frac{\varepsilon'}{\varepsilon'^2 + \varepsilon''^2}\right] \qquad (2)$$

where C_0 is the capacitance of vacuum.

III. Results and Discussion

XRD patterns of the Pr-doped $SrBi_2Nb_2O_9$ ceramic powers are shown in Fig. 1. All the spectra show well-defined peak reflections corresponding to orthorhombic (space group A21am) phase according to the JCPDS card, without forming any secondary phases. The high intensity of the diffraction peak (115) is shifted from 29.03° for the undoped sample to 28.97° for the doped sample. Table 1 summarizes the XRD data parameters of the Pr-doped $SrBi_2Nb_2O_9$. It can be seen that the values of the volume and lattice parameters have increased with Pr doping. The orthorhombic distortion (b/a), and orthorhombicity [2|a-b|/(a+b)] were found to decrease, confirming the distortion of the Nb_2O_6 octahedral [10]. The observed results could be related to the incorporation of praseodymium ions on Bi^{3+} sites in Bi_2O_2 layers. The crystallite size was calculated using the Debye-Scherrer formula:

$$D = \frac{0.9\lambda}{\beta \cos\theta} \qquad (3)$$

where β is a half-width of the peak and λ = 1.5406 Å is the wavelength of CuKα radiation. The crystallite size varies from 20 nm for x = 0 to 25 nm for x = 0.2. All these results indicate that Pr ions may have diffused in the lattice structure.

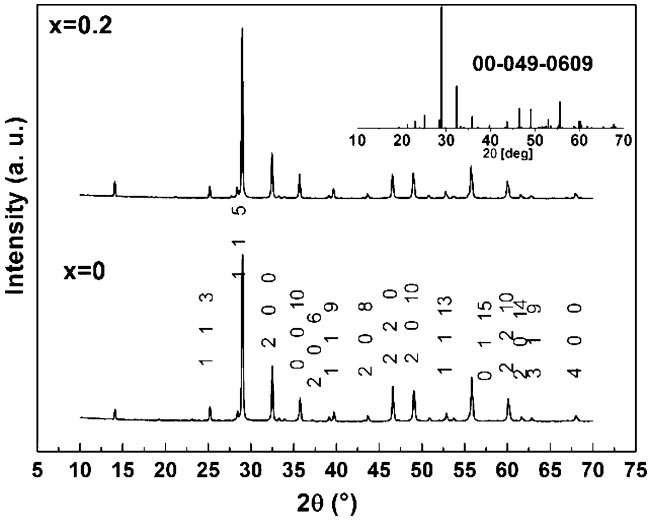

Fig. 1: XRD patterns of $SrBi_{2-x}Pr_xNb_2O_9$ ceramic powders.

Fig. 2 shows SEM images of the Pr-doped $SrBi_2Nb_2O_9$ ceramics. Plate-like grains are observed for the undoped ceramics with a mean grain size of 1 μm in width and 0.2 μm in thickness. The plate-like morphology is the characteristic feature of Aurivillius phases [11, 12]. However, rod- and plate-like grains are obtained for the doped ceramics with the mean grain size is 0.75 μm. The undoped ceramic is denser than the doped ceramic. This is shown by the x = 0 micrograph in Fig. 2. In addition, the x = 0.2 micrograph reveals the presence of porosity, indicating that the sintering conditions are not optimal to achieve a dense ceramic. The crystallite size results from the Scherrer equation are not consistent with the micrographs. The average crystallite size estimated from the XRD data is found to be around nanoscale, unlike in the SEM micrographs, which showed the presence of micrograins. In addition, the seemingly very different densities do not allow the true effect of the Pr to be separated from the effect of density.

Fig. 3 shows the frequency dependence of the dielectric constant (ε') and dielectric loss ($tan\delta$) for Pr-doped $SrBi_2Nb_2O_9$ ceramics. As frequency increases, the dielectric constant of undoped sample decreases dramatically. The different electric dipoles having different relaxation frequencies and the conductivity cause the dielectric constant of the material to decrease dramatically.

Table 1: XRD data of $SrBi_{2-x}Pr_xNb_2O_9$ ceramic powders.

	x = 0	x = 0.2
a (Å)	5.5023	5.5092
b (Å)	5.5083	5.5117
c (Å)	25.0985	25.1439
cell vol (Å^3)	760.6978	763.5055
2|a-b|/(a+b)	0.0011	0.0005
b/a	1.0011	1.0005
D (nm)	25	24

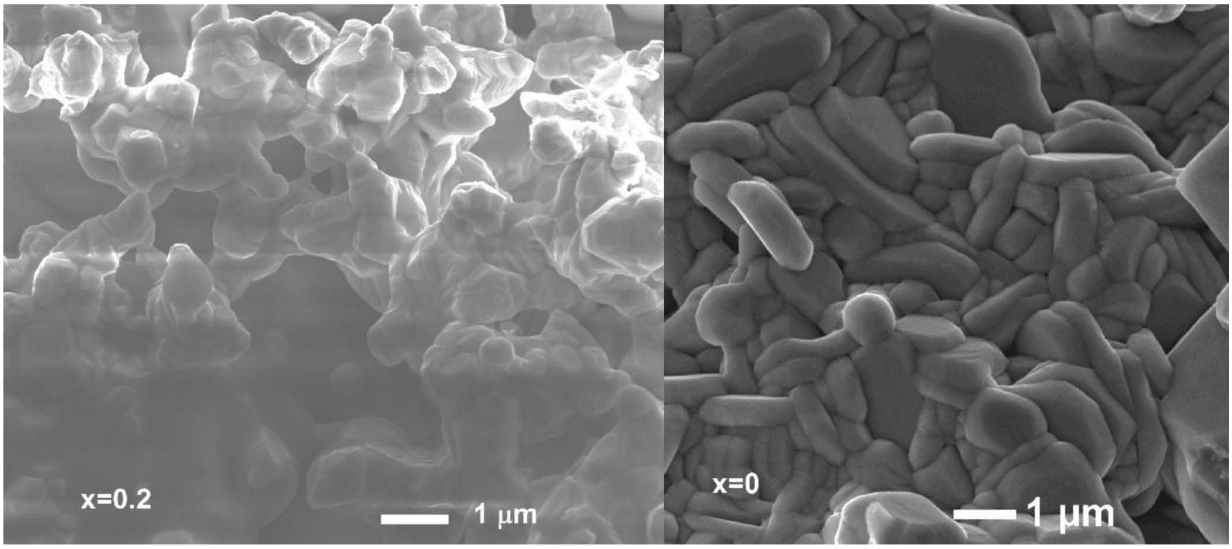

Fig. 2: SEM images of $SrBi_{2-x}Pr_xNb_2O_9$ ceramics.

However, ε' remains constant as the frequency is increased for the doped sample. At higher frequency (insert graph), the response from Pr-doped $SrBi_2Nb_2O_9$ becomes higher than that of $SrBi_2Nb_2O_9$. The Pr-doped $SrBi_2Nb_2O_9$ sample has a dielectric constant of around 133 when it is measured at 1 MHz, which is about 43 higher than that of $SrBi_2Nb_2O_9$. With reference to Fig. 3, the evolution of the dielectric loss as a function of frequency is the same as ε'-*Frequency* plots. The dielectric loss of the undoped ceramic is several times more than that of the doped ceramic. It is found to be 0.17 and 0.02 respectively for the undoped and doped ceramics when these are measured at 10 kHz. Note also the two curves converge at the high frequencies (< 100 kHz), the value of the dielectric loss is estimated to be 0.02 and 0.015 respectively for the undoped and doped ceramics when these are measured at 1 MHz.

The high dielectric constant could be interpreted as an extrinsic mechanism, which was assumed to come from the sample microstructure such as boundary or interface effects[13]. Thus, the holes in a solid dielectric offer little resistance to electrical breakdown, causing the very rapid decline in dielectric strength with increasing porosity [14]. In our experimental results, the undoped sample, which has a denser microstructure than that of the doped sample, as can be seen from Fig. 3, exhibits the lower dielectric constant at higher frequencies. This result is in contradiction to those reported in the literature, which reveal that the dielectric properties may be improved by increasing the density of ceramics. On the other hand, the relative amount of the Pr^{3+} and Pr^{4+} electronic state concentrations present in the sample could lead to an increase in the hopping electrons that are oriented in the direction of the applied field, causing an increase in the dielectric polarization. Additionally, we observed changes in the color of the Pr-doped $SrBi_2Nb_2O_9$ ceramic from colorless (before sintering) to spring green (after sintering), confirming the presence of the Pr^{3+}/Pr^{4+} couple. Referring to the ferrite materials, the electronic exchange between ferrous and ferric ions (Fe^{2+}/Fe^{3+}). The dielectric behaviour of the ferrites was attributed to the mechanism of the polarization process arising from the electronic exchange between Fe^{2+} and Fe^{3+} [15, 16]. On the basis of the above, the high dielectric constant at room temperature is due in particular to the activity of charge carriers resulting from the electron exchange between Pr^{3+} ions and Pr^{4+} ions.

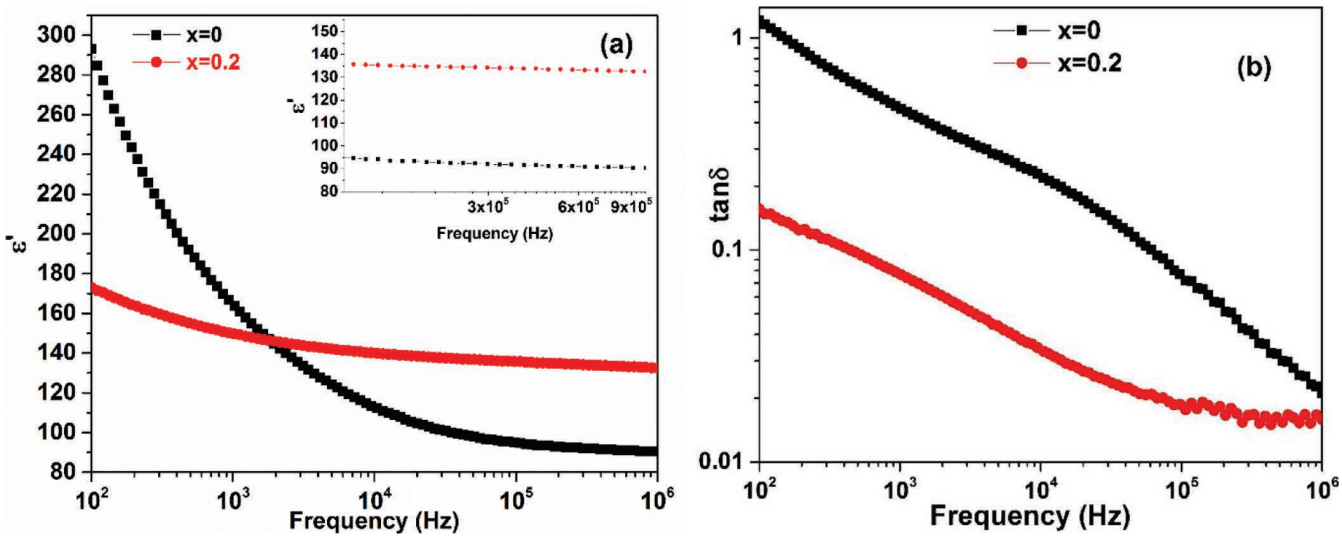

Fig. 3: Frequency dependence of dielectric constant (ε′) and dielectric loss (tan δ) for $SrBi_{2-x}Pr_xNb_2O_9$ ceramics at room temperature.

Fig. 4 shows the variation of AC conductivity as a function of frequency at room temperature for Pr-doped $SrBi_2Nb_2O_9$ ceramics. The AC conductivity of both samples increases with frequency and then converges at high frequency. It is found to be in the order of 10^{-6}–$10^{-4}\ \Omega^{-1}m^{-1}$ in all the samples, indicating that the oxygen ion vacancies might be the responsible charge carrier species in the conductive mechanism [17]. Meanwhile, the AC conductivity of the undoped ceramic is twice that of the doped ceramic when this is measured at a frequency lower than 100 kHz. Taking into consideration chemical bond, the bond dissociation energy (enthalpy change) for a bond Pr-O broken during sintering is 753 kJ/mol (Pr-O), and for Bi-O it is 343 kJ/mol (Bi-O) [18]. The presence of supplementary bonding (Pr-O) in the crystal could hamper the formation of oxygen vacancies arising from the volatilization of bismuth when the material is exposed to the sintering process, because Pr-O is not easily broken. Moreover, the occupation of an oxygen vacancy site by a praseodymium ion could reduce the electron trap sites. These dual roles of the praseodymium-doping (reduction of electron trap sites and oxygen ion vacancies) lead to a reduction in the value of AC conductivity. However, the highly polarized Bi^{3+} cations and weak Bi–O bonds are helpful for the migration of oxygen ions, leading to higher AC conductivity [19].

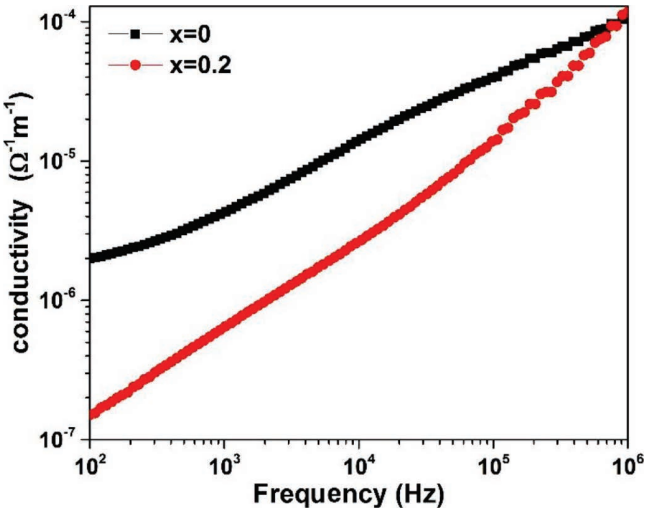

Fig. 4: Plot of AC conductivity versus frequency for $SrBi_{2-x}Pr_xNb_2O_9$ ceramics at room temperature.

The frequency dependence of the complex impedance at room temperature of Pr-doped $SrBi_2Nb_2O_9$ ceramics is shown in Fig. 5. The Z′ versus Z″ plot reveals a single semi-circle for x = 0 and an uncompleted arc for x = 0.2. The equivalent circuit model is interpreted as the parallel combination of R_p (resistance) and CPE (Constant Phase Element) in series with R_s (resistance) as shown in the inset figure. The diameter of the semi-circle of the doped ceramic is much larger than that of the undoped ceramic, owing to the development of porosity [20], which is corroborated in the SEM results. Taking in consideration the internal microstructure, the grain boundary resistance decreases with the decreasing semi-circle diameter in the Z' versus Z' ' plot. This is due to the grain boundary effect, which has assisted in lowering the barrier to the motion of charge carriers [21]. The grain boundary involves an energetic barrier which separates the grains. Thus, this potential barrier opposes the migration of electron transfer between Pr^{3+} and Pr^{4+} ions in grains. It is accompanied by a small eddy current, hence the decrease in the dielectric loss in Pr-doped ceramic. In contrast, $SrBi_2Nb_2O_9$ shows a smaller decrease because of the diameter of the semi-circle and therefore its good conductivity [22].

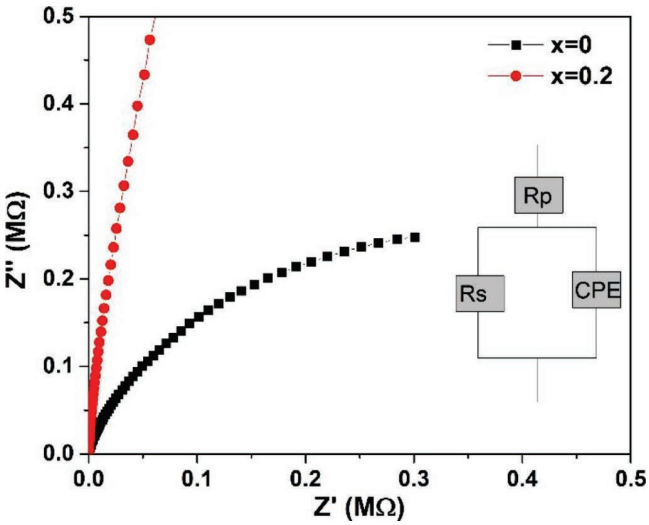

Fig. 5: Z′ versus Z″ plot for $SrBi_{2-x}Pr_xNb_2O_9$ ceramics at room temperature.

IV. Conclusions

This manuscript reports on the structural and dielectric properties of Bi-based Aurivillius layered-structure oxides prepared with a solid-state method. The dielectric polarization created by the exchange of electrons between Pr^{3+} and Pr^{4+} could be the origin of the higher dielectric constant. Therefore, in contrast to the doped phase of praseodymium oxide, the phase contains intrinsic oxygen vacancies. These oxygen vacancies are disordered throughout the lattice, yielding a conductivity approximately. A dopant such as Pr, which has been introduced into $SrBi_2Nb_2O_9$ to help stabilize the phase, will reduce the number of oxygen ion vacancies available for the conduction process. The flattening of the dielectric constant at high frequencies with lower dielectric loss means that Pr-doped $SrBi_2Nb_2O_9$ material can be considered as a candidate for FeRAM applications.

References

1 Zou, H., Yu, Y., Li, J., Cao, Q., Wang, X., Hou, J.: Photoluminescence, enhanced ferroelectric, and dielectric properties of Pr^{3+}-doped $SrBi_2Nb_2O_9$ multifunctional ceramics, *Mater. Res. Bull.*, **69**, 112 – 115, (2015).

2 Kannan, B.R., Venkataraman, B.H.: Influence of samarium doping on structural and dielectric properties of strontium bismuth tantalate ceramics derived by molten salt synthesis route, *J. Mater. Sci. Mater. Electron.*, **25**, 4943 – 4948, (2014).

3 Lin, S., Jun-hao, C., Ping-xiong, Y., Fang-Yu, Y., Ya-Wei, L., Chu-De, F., Cao-Liang, M.: Influence of substitution of Nd^{3+} for Bi^{3+} on structure and piezoelectric properties of $SrBi_{2-x}Nd_xNb_2O_9$ (x = 0, 0.1, 0.2 and 0.4), *Trans. Nanoferrous Met. Soc. China*, **19**, 1459 – 1463, (2009).

4 Afqir, M., Tachafine, A., Fasquelle, D., Elaatmani, M., Carru, J.-C., Zegzouti, A., Daoud, M.: Dielectric properties of gadolinium-doped $SrBi_2Nb_2O_9$ ceramics, *J. Mater. Sci. Mater. Electron.*, 1 – 9, (2017).

5 Huang, S., Feng, C., Chen, L., Wen, X.: Dielectric properties of $SrBi_{2-x}Pr_xNb_2O_9$ ceramics (x=0, 0.04 and 0.2), *Solid State Commun.*, **133**, 375 – 379, (2005).

6 Zou, H., Yu, Y., Li, J., Cao, Q., Wang, X., Hou, J.: Photoluminescence, enhanced ferroelectric, and dielectric properties of Pr^{3+}-doped $SrBi_2Nb_2O_9$ multifunctional ceramics, *Mater. Res. Bull.*, **69**, 112 – 115, (2015).

7 Suárez, D.Y., Reaney, I.M., Lee, W.E.: Relation between tolerance factor and tc in aurivillius compounds, *J. Mater. Res.*, **16**, 3139 – 3149, (2001).

8 Sugandha, S., Jha, A.K.: Effect of holmium substitution on electrical properties of strontium bismuth tantalate ferroelectric ceramics, *Ceram. Int.*, **39**, 9397 – 9403, (2013).

9 Afqir, M., Tachafine, A., Fasquelle, D., Elaatmani, M., Carru, J.C., Zegzouti, A., Daoud, M.: Dielectric properties of $SrBi_{1.8}RE_{0.2}Nb_2O_9$ (RE = Yb, Tm, Tb, Gd, Er, Sm and Ce) ceramics, *Solid State Sci.*, **73**, 51 – 56, (2017).

10 Singh, R., Luthra, V., Rawat, R.S., Tandon, R.: Structural, dielectric and piezoelectric properties of $SrBi_2Nb_2O_9$ and $Sr_{0.8}Bi_{2.2}Nb_2O_9$ ceramics, *Ceram. Int.*, **41**, 4468 – 4478, (2015).

11 Senthil, V., Badapanda, T., Chandrabose, A., Panigrahi, S.: Dielectric and ferroelectric behavior of cerium modified $SrBi_2Ta_2O_9$ ceramic, *Mater. Lett.*, **159**, 138 – 141, (2015).

12 Keeney, L., Kulkarni, S., Deepak, N., Schmidt, M., Petkov, N., Zhang, P.F., Cavill, S., Roy, S. *et al.*: Room temperature ferroelectric and magnetic investigations and detailed phase analysis of aurivillius phase $Bi_5Ti_3Fe_{0.7}Co_{0.3}O_{15}$ thin films, *J. Appl. Phys.*, **52010**, 1 – 11, (2012).

13 Khasa, S., Singh, P., Sanghi, S., Singh, N., Agarwal, A.: Structural analysis and dielectric characterization of aurivillius type $CaSrBi_2Nb_2O_9$ ceramics, *J. Integr. Sci. Technol.*, **2**, 13 – 21, (2004).

14 Gerson R., Marshall, T.C.: Dielectric breakdown of porous ceramics, *J. Appl. Phys.*, **30**, 1650 – 1653, (1959).

15 Ranga Mohan, G., Ravinder, D., Ramana Reddy, A.V., Boyanov, B.S.: Dielectric properties of polycrystalline mixed nickel-zinc ferrites, *Mater. Lett.*, **40**, 39 – 45, (1999).

16 Kharabe, R.G., Jadhav, S.A., Shaikh, A.M., Patil, D.R., Chougule, B.K.: Magnetic properties of mixed li-ni-cd ferrites, *Mater. Chem. Phys.*, **72**, [1], 77 – 80, (2001).

17 Palanduz, A.C., Smyth, D.M.: Defect chemistry and charge transport in $SrBi_2Nb_2O_9$, *J. Electroceramics*, **11**, 191 – 206, (2003).

18 Cottrell, T.L.: The Strengths of Chemical Bond, 2nd edn. Butterworth, London, (1958).

19 Li, M., Pietrowski, M.J., De Souza, R.A., Zhang, H., Reaney, I.M., Cook, S.N., Kilner, J.A., Sinclair, D.C.: A family of oxide ion conductors based on the ferroelectric perovskite $Na_{0.5}Bi_{0.5}TiO_3$, *Nat. Mater.*, **13**, 31 – 35, (2013).

20 Li, X., Cao, X., Xu, L., Liu, L., Wang, Y., Meng, C., Wang, Z.: High dielectric constant in Al-doped ZnO ceramics using high-pressure treated powders, *J. Alloy. Compd.*, **657**, 90 – 94, (2016).

21 Krishnan, V.G., Elango, P., Ragavendar,M., Sathish, P., Gowrisankar, G.: Effect of post annealing on the band gap of $Mg_xZn_{1-x}O$ thin films, *Mater. Res. Express*, **4**, 036401: 1 – 5, (2017).

22 Khan, M.E., Khan, M.M., Cho, M.H.: Ce^{3+}-ion, surface oxygen vacancy, and visible Light-induced photocatalytic dye degradation and photocapacitive performance of CeO_2-graphene nanostructures, *Sci. Rep.*, **7**, 5928, (2017).